



CHORUS

This is the accepted manuscript made available via CHORUS. The article has been published as:

Deposition of cobalt atoms onto Alq₃ films: A molecular dynamics study

Yun-Peng Wang, Xiu-Feng Han, James N. Fry, Jeffrey L. Krause, X.-G. Zhang, and Hai-Ping Cheng

Phys. Rev. B **90**, 075311 — Published 28 August 2014

DOI: [10.1103/PhysRevB.90.075311](https://doi.org/10.1103/PhysRevB.90.075311)

Deposition of metal atoms onto organic thin film: a molecular dynamics study

Yun-Peng Wang and Xiu-Feng Han

*Beijing National Laboratory of Condensed Matter Physics,
Institute of Physics, Chinese Academy of Sciences, Beijing 100190, China*

James N. Fry and Jeffrey L. Krause

*Quantum Theory Project, University of Florida, Gainesville, Florida 32611, USA and
Department of Physics, University of Florida, Gainesville, Florida 32611, USA*

X.-G. Zhang

*Center for Nanophase Materials Sciences and Computer Science and Mathematics Division,
Oak Ridge National Laboratory, P. O. Box 2008, Oak Ridge, Tennessee 37831-6493, USA*

Hai-Ping Cheng

*Department of Physics, University of Florida, Gainesville, Florida 32611, USA and
Quantum Theory Project, University of Florida, Gainesville, Florida 32611, USA*

The charge and spin injections into semiconductors are determined by the quality of electrode/semiconductor interface. The latter is defined by the atomic penetration depth when growing metal electrodes on organic semiconductor thin films by physical deposition method. Although the interfaces between top electrodes and a typical organic material, tris(8-hydroxyquinoline) aluminum (Alq_3) thin films have been intensively investigated by several groups, their results on the atomic penetration depth into Alq_3 film diverged from each other. In this paper, we studied the deposition of cobalt atoms onto Alq_3 thin films using the molecular dynamics method. The intermixing between Co and Alq_3 is calculated to be limited to the first Alq_3 layer for low Co initial kinetic energies, but spread to a few layers for high initial energies. Our calculation results indicate that proper deposition method with low injection energy helps to reduce the amount of intermixing at interfaces and to improve the magnetoresistance of organic-based magnetic junction.

PACS numbers: 36.40.Sx, 68.35.Fx, 61.46.-w

I. INTRODUCTION

Devices based on organic molecules such as organic light emitting diodes¹ and organic spin valves² have gained wide interest. Most of these devices have a multi-layer structure, with an organic thin film sandwiched between bottom and top metal electrodes.^{1,2} Deposition of the top metal electrode onto the organic thin film is often the most difficult step in device preparation, because deposited metal atoms with high initial kinetic energy can penetrate into the organic thin film and form a metallic path connecting top and bottom electrodes.²

Studies of the deposition of noble metal atoms onto organic self-assembled monolayers (SAMs) have shown that terminal groups of molecules play a critical role: molecules with reactive terminal groups prevent, while inert terminal groups favor, penetration of metal atoms into SAMs.³⁻¹⁰ Penetration of gold atoms into alkanethiol SAMs was reproduced by molecular dynamics simulations,¹¹ which also revealed differing dynamical behaviors for silver clusters of different sizes on alkanethiol SAMs.¹² Deposition of calcium and aluminum atoms on self-assembled poly(*para*-phenylene vinylene) (PPV) surfaces were numerically simulated by Giro *et al.*^{13,14} using the molecular dynamics method.

Concerning spintronics devices, the interface between ferromagnetic metals and organic films, especially cobalt

atop amorphous Alq_3 thin films, has attracted much interest after observation of giant magnetoresistance in LSMO/ Alq_3 /Co magnetic junctions² and in other organic spin valves^{15,16} Bad interface caused by atom penetration is the main reason for controversy on the sign and the mechanism of the magnetoresistance in Alq_3 -based spin valves.¹⁷ The electric current carrier injection efficiency from magnetic electrodes into Alq_3 thin film spacer was fitted by modified space charge limited current model to be different for interfaces grown by different methods.¹⁷ For this reason, the penetration of metal atoms into Alq_3 thin film has been extensively investigated by several groups but their results diverged with each other. Xiong *et al.*² observed that magnetoresistance exponentially decays as a function of the thickness of Alq_3 space layers, but observed no magnetoresistance when the thickness of Alq_3 was less than 100 nm. They argued an “ill-defined” interface with thickness of 87 nm owing to interdiffusion exists between cobalt and Alq_3 . Vinzelberg *et al.*¹⁸ used electron energy lose spectroscopy (EELS) to detect intensity profile of cobalt element along a line perpendicular to Alq_3 /Co interface and confirmed inclusion of cobalt atom in Alq_3 with distance up to 50 nm. In contrast to Refs. 2 and 18, Santos *et al.*¹⁹ measured the spin-polarization of the tunnel current from cobalt, iron, and permalloy through an Alq_3 barrier into superconducting aluminum and argued that the Alq_3

barrier is free from cobalt inclusions. X-ray and ultraviolet photoelectron spectra of Alq₃/Co thin films provided strong evidence of abrupt interface of cobalt atop of Alq₃ thin films.²⁰ The intermixing or diffusion of Co into Alq₃ was observed to be limited and the interface width was measured by high resolution transmission electron microscopy (TEM) to be similar to surface roughness of Alq₃ thin film.²¹ These controversial results reflect difficulties in preparing devices with clean and sharp Alq₃/Co interfaces. A detailed study on surface topographies of bare Alq₃ thin films and Co/Alq₃ bilayers revealed that self-grown pinholes in Alq₃ thin film and pinholes induced by substrates other than Co inclusions are the reason for ill-defined interface.²²

Interactions between cobalt atoms and Alq₃ molecules were also investigated. Cobalt-doped Alq₃ thin films prepared by thermal co-evaporation exhibit ferromagnetic behavior with a magnetization of $\sim 0.33 \mu_B$ per cobalt atom.²³ Density functional theory with the generalized gradient approximation (GGA) was used to reproduce the ferromagnetic exchange interaction between cobalt dopants, and it was found that there is strong attraction between the aromatic ring in Alq₃ molecules and cobalt atoms.²⁴ However, investigations of the dynamical process of cobalt atoms or clusters depositing onto Alq₃ films is still lacking.

The aim of this paper is to try to answer this question: Does cobalt penetrate deeply into Alq₃ films? In the paper, we present our numerical simulations on deposition of cobalt atoms onto amorphous Alq₃ thin films. Cobalt atoms instead of clusters were used in this study. Large metal clusters are believed to penetrate more weakly than atoms into soft substrates,¹⁷ so the penetration depth of cobalt atoms into Alq₃ thin films should give the upper limit of Alq₃/Co interface thickness due to intermixing. From our numerical simulations, we obtained statistics of penetration depth and dependence on the initial kinetic energy of the cobalt atom. With low initial energies, cobalt atoms stay at the Alq₃ surface. Cobalt atoms can penetrate into Alq₃ thin film with higher initial energies, with a penetration depth limited to a few nanometers. The microscopic process of one cobalt atom colliding with an Alq₃ thin film was visualized and we found 8-hydroxyquinoline ligands perpendicular to velocity of cobalt atom stop the penetration of the cobalt atom.

The paper is organized as following: In Section II, computational details, in particular the construction of the force field to describe interaction between Alq₃ and cobalt atoms are presented. Molecular dynamics simulation results, especially statistics on penetration depth of cobalt atom into Alq₃ film are also presented in the same section. In Section III, the microscopic collision process of a cobalt atom with an Alq₃ molecule is analyzed. In addition, charge transfer and orbital hybridization between Alq₃ and an adjacent cobalt atom were obtained using density functional method. Section IV contains a summary.

II. SYSTEM AND SIMULATION RESULTS

The quality of the force field describing metal-molecule interactions is very important to determine whether injected metal atoms penetrate into molecular films or not. Alkis *et al.*¹¹ used a Lennard-Jones potential with energy parameter scaled by a factor of 5 and 10 to describe alkanethiol-Au interaction, because the unmodified Universal Force Field (UFF)²⁵ was found to give a binding energy ten times smaller than that in first-principles calculations. They found that Au atoms penetrate into self-assembled alkanethiol monolayer if the potential well of the alkanethiol-Au interaction is deep.¹¹ Because of the relatively large amount of charge transfer from reactive metallic elements to organic polymers, the charge-equilibration method²⁶ was used to describe interactions between reactive metals (Ca and Al) and poly(*para*-phenylene vinylene).^{13,14} However, we found that the Alq₃-Co binding energy was also underestimated by the charge-equilibration method²⁶ compared to our first-principle calculation results.

We thus used a method similar to that of Ref. 11 to construct a force field describing Alq₃-Co interactions. Binding energies of 72 different Alq₃-Co configurations were obtained by first-principle calculations. Density functional theory²⁷ implemented in the QUANTUM ESPRESSO package²⁸ was used. The Perdew-Burke-Ernzerhof parameterization²⁹ of the generalized gradient approximation on the exchange-correlation functional was used. Interaction between valence electrons and ions were described by projector augmented-wave^{30,31} datasets. Wave functions are expanded using plane-waves, and kinetic energy cutoffs of 500 eV and 6,000 eV were used for wave functions and charge density, respectively. In order to perform Bader charge analysis³², all-electron charge density was recovered from calculations. In these calculations, the Alq₃ molecule was kept fixed and the cobalt atom was placed at various locations around the Alq₃ molecule. Configurations of Alq₃-Co clusters were categorized into two groups, one in which the cobalt atom was put on a line perpendicular to and through the center of an aromatic ring and one through a N(O)-triangle. When the cobalt atom is located near the center of an aromatic ring in an 8-hydroxyquinoline ligand, the binding energy is calculated to be 1.4–2.0 eV, but only 1.0–1.3 eV when near an N(O)-triangle. This result indicates cobalt atom prefer to be adsorbed near aromatic rings rather than near oxygen or nitrogen atoms, which is consistent with previous first-principle calculation result²⁴.

The Lennard-Jones potential, with the form $U(r_{ij}) = 4\epsilon[(\sigma/r_{ij})^{12} - (\sigma/r_{ij})^6]$, was chosen to fit the first-principle binding energies in different configurations. Optimized Lennard-Jones parameters for Alq₃-Co interactions used in this work are listed in Table I. The Lennard-Jones potential and the first-principles binding energies for a cobalt atom located on a line perpendicular to and through the center of an aromatic ring and a O(N)-

triangle are plotted in Fig. 1. The potential well depth and shape are well reproduced by the Lennard-Jones potential with optimized parameters. The force field of Alq₃ molecules was constructed following the same procedure used in Ref. 33.

TABLE I. Optimized Lennard-Jones parameters for Alq₃-Co interactions. The pairwise Lennard-Jones potential between atoms takes the form $U(r_{ij}) = 4\epsilon [(\sigma/r_{ij})^{12} - (\sigma/r_{ij})^6]$ where ϵ and σ are energy and length scale parameters and r_{ij} is inter-atomic distance.

	Co-C	Co-O	Co-Al	Co-H	Co-N
σ (Å)	1.78	1.96	1.78	1.78	1.96
ϵ (kcal/mol)	6.92	4.61	2.31	4.61	2.31

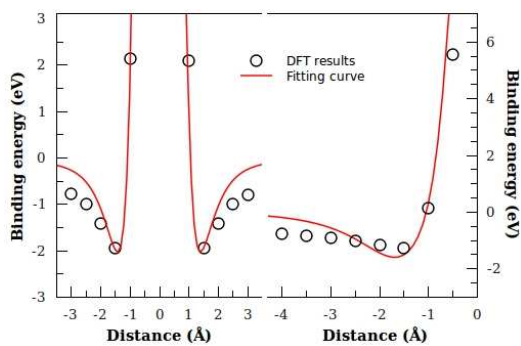


FIG. 1. Optimized Lennard-Jones potential (solid lines) and first-principle binding energies (circles) along two lines perpendicular to and through the center of an aromatic ring (left) and of a N(O)-triangle (right).

Our model system consists of an amorphous Alq₃ thin film with average thickness about 4.2 nm. The unit cell of the system is a rhombus with side 5.0 nm, repeated in the x - y plane. The amorphous Alq₃ thin film was prepared using a two-stage strategy. 128 Alq₃ molecules were initially put on a regular lattice with random orientations, in analog to a high-temperature annealing process. At the second stage, a molecular dynamics simulation in the canonical (NVT) ensemble with Berendsen thermostat at temperature of 300 K was used until the total energy reaches equilibrium. The prepared amorphous Alq₃ thin film has a density of 1.25 g/cm³, which is close to the experimental density.

Because of the roughness of the amorphous Alq₃ surface, the penetration depth of a cobalt atom can not be directly determined by its final position alone, but the topography of the Alq₃ surface is also needed. One can imagine a cobalt atom moving from $(x, y, z = +\infty)$ downwards towards the Alq₃ surface along a line perpendicular to the x - y plane with infinitesimal kinetic energy. If the x - y position of the cobalt atom is constrained, the final position of the cobalt atom would be the first energy minimum it encounters. As a result, the surface of

the Alq₃ thin film at (x, y) can be defined as the position of the energy minimum with the highest z . There are also other possible definitions for the surface, such as the location with the same potential energy or with the same potential energy derivative. The atomic force microscopy (AFM) technique belongs to the latter category, whereas our definition has no parameters. Based on our definition, the topography of the Alq₃ surface can be illustrated by an AFM-like image, as shown in Fig. 2. The root-mean-square roughness of the Alq₃ surface is 0.3 nm, and its peak-to-peak roughness is 2.0 nm, values close to those observed in experiments.^{34,35} The Alq₃ thin film used in our simulation is free from pinholes²² or small grains^{35,36}. As a result, the filling of Co atoms into pinholes in Alq₃ thin film cannot be taken account for by our simulations.

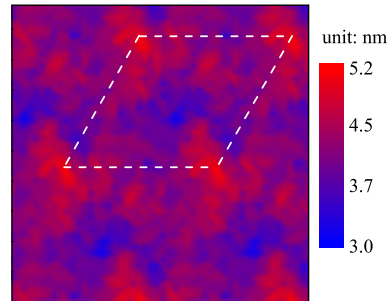


FIG. 2. (Color online) A 10×10 nm² AFM-like image of the surface of the Alq₃ thin film, with root-mean-square roughness 0.3 nm and peak-to-peak roughness 2.0 nm. The white dashed rhombus shows the unit cell of our model system.

After preparing the Alq₃ thin film, cobalt atoms were projected onto the film. The initial velocity of cobalt atom was along the $-z$ direction, towards the Alq₃ surface. Initial positions for 200 cobalt atoms were generated randomly starting far away from the Alq₃ surface. For each initial position, four trajectories with initial kinetic energies of 0.15, 1, 5 and 10 eV to simulate different deposition methods used in experiments were followed using molecular dynamics. The kinetic energy of cobalt atoms deposited by the thermal evaporation method has a narrow distribution³⁷ with the most probable energy of 0.15 eV ($k_B T_b \approx 0.15$ eV, where k_B is the Boltzmann constant and $T_b = 1768$ eV is the boiling temperature of Co). In contrast, the kinetic energy of a cobalt atom deposited by the sputter method has a much wider distribution³⁷, with a most probable energy of 5 eV. Initial kinetic energies of 1, 5 and 10 eV were chosen to model a low energy, the most probable energy, and a high energy. The molecular dynamics simulation was performed using the DL_POLY³⁸ program with a time step of 0.2 fs. Each trajectory ended after 3–4 ps, when the cobalt atom touches the Alq₃ surface. We are particularly interested in the energy exchange between Co atom and Alq₃ thin film at the initial stage of Co deposition process. Concerning that significant energy transfer

from Co atom to Alq₃ thin film happens in a short time (3–4 ps), we neglect the relaxation of total energy during our simulations. The microcanonical ensemble was used to simulate the Co deposition process, namely the total energy (kinetic energy plus configuration energy) is kept constant.

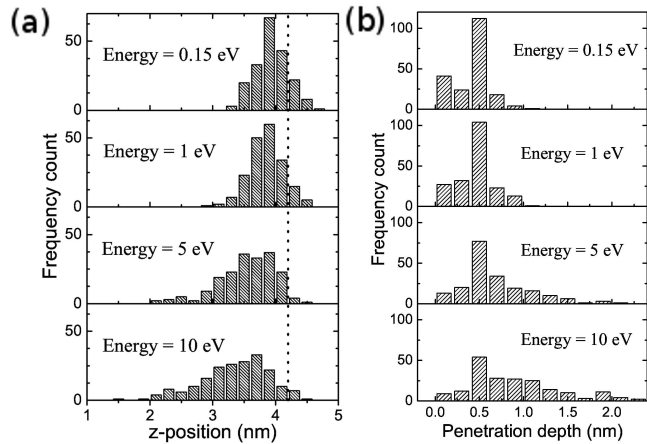


FIG. 3. (a) Frequency distribution of the z -component of final position, and (b) penetration depth of cobalt atoms for different initial energies. The dotted line in (a) shows the average height of the Alq₃ thin film.

Statistics of the final z -positions of cobalt atoms are shown in Fig. 3(a). If the initial kinetic energy of the cobalt atom is 0.15 eV, the distribution of final positions is almost symmetrically centered at $z = 3.9$ nm, which is about 0.4 nm below the average height of the Alq₃ thin film. When the initial kinetic energy of the cobalt atom increases to 1 eV, the distribution of final positions becomes asymmetric and a slight small- z tail develops, indicating the beginning of cobalt penetration into the Alq₃ film. When the initial kinetic energy of the cobalt atom is 5 eV, or even higher at 10 eV, the small- z tail in final position extends further, as shown in the last two panels of Fig. 3(a). Penetration depth is calculated as the difference between the z -component of the final position of the Co atom and the local height of the Alq₃ film. Statistics of penetration depth are shown in Fig. 3(b). The cobalt atom can penetrate into the Alq₃ film if its initial kinetic energy is large. However, even with the largest initial energy the penetration depth is limited to about 2 nm.

The penetration depth of cobalt atom is not restricted by the thickness of Alq₃ film. We performed a simulation with a 2 nm thick Alq₃ film and found that a small portion of cobalt atoms penetrate the whole Alq₃ film. In contrast, no cobalt atom penetrate the whole 4 nm thick Alq₃ film. We also examined the correlation between Alq₃ surface height and penetration depth of cobalt atoms for different initial energies, and found that the distribution of cobalt penetration depths are independent of Alq₃ surface height, which indicates that the cobalt atoms penetrate into Alq₃ uniformly.

The intermixing of Co atoms and Alq₃ molecules at the Alq₃/Co interface was observed by our numerical simulations. Given that the size of Alq₃ molecule is about 1 nm, it is observed that Co atoms with low initial energy, or grown by thermal evaporation method mix with Alq₃ molecules in the first layer. For Co atoms grown by sputter method and with higher initial energies, the intermixing of Co atoms and Alq₃ molecules spreads to the second Alq₃ layer. The simulation results indicate that the intermixing at interface cannot be avoided. On the other hand, the intermixing is limited to a few layers of Alq₃ molecules even if Co atoms were deposited by sputter method. The intermixing at interface inevitably affect the charge and spin injection into Alq₃ thin film, hence any theory trying to explain the transport properties of organic-based magnetic junctions should consider this factor.

III. DISCUSSION

The microscopic collision process between a cobalt atom and the Alq₃ surface can be studied by looking into one trajectory in detail. One Alq₃ molecule has three mutually perpendicular 8-hydroxyquinoline ligands connected to the Al atom by O and N atoms. A ligand that lies parallel to z -axis would fail to stop the penetration of cobalt atom with high velocity. However, a cobalt atom stops penetrating further after collision with a ligand parallel to the x - y plane. During the collision of cobalt atom with Alq₃ thin film, the local temperatures of Alq₃ molecules near the cobalt atom trajectory increase. In order to show the collision process clearly, only Alq₃ molecules with local temperatures higher than a threshold value T_{thr} are shown. Local temperature T of one Alq₃ molecule is defined by the kinetic energy as

$$\frac{f}{2}k_{\text{B}}T = \frac{1}{2} \sum_i m_i \vec{v}_i^2 \quad (1)$$

where k_{B} and f are the Boltzmann constant and the total number of freedom for one Alq₃ molecule, and m_i and \vec{v}_i are mass and velocity of i th atom in the Alq₃ molecule. Temperature of one atom is defined in the same manner with $f = 3$.

In Fig. 4, snapshots of one trajectory with initial energy 10 eV and penetration depth 1.5 nm are shown. Because local temperatures (kinetic energies) of atoms in Alq₃ molecules increase after collision with the projectile cobalt atom, local temperatures of atoms in Alq₃ molecule are illustrated by different colors, which helps us to understand the energy transfer from cobalt atom to Alq₃ molecules. At 1.6 ps, the cobalt atom has touched one 8-hydroxyquinoline ligand of the Alq₃ molecule, as shown in Fig. 4(a). This ligand, parallel to the z -axis, failed to stop the cobalt atom with high velocity; however, the ligand was heated due to its interaction with the cobalt atom. The cobalt atom next hits a ligand in

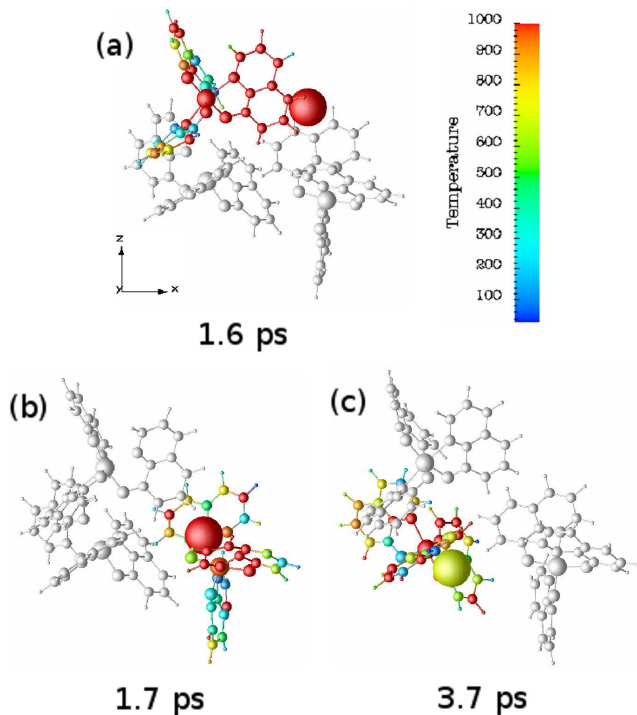


FIG. 4. (Color Online) Snapshots at (a) 1.6 ps, (b) 1.7 ps and (c) 3.7 ps of one trajectory with initial energy of 10 eV and penetration depth of 1.5 nm. The largest sphere in each snapshot represents the cobalt atom. Three Alq₃ molecules adjacent to trajectory of the cobalt atom are shown in each snapshot. Atoms of the Alq₃ molecule, which is directly interacted with the cobalt atom, are in different colors according to their local temperatures. The other two Alq₃ molecules are in light gray in order to make the figures clear. Atoms in Alq₃ molecules are illustrated by spheres with radii $\text{Co} > \text{Al} > \text{O} > \text{N} > \text{C} > \text{H}$. Local temperatures of atoms are defined by Eq. (1). Coordinate system orientations for (a)-(c) are the same.

a second Alq₃ molecule which is not parallel to z -axis, as shown in Fig. 4(b). The direction of the cobalt atom velocity was changed by collision with this ligand, and it now moves in the x - y plane instead of penetrating further. Finally, at 3.7 ps, the cobalt atom has found its most stable adsorption site, near a third Alq₃ molecule as shown in Fig. 4(c). This microscopic analysis shows that collision of a cobalt atom with 8-hydroxyquinoline ligand not parallel to the z -axis would stop its penetration. Because each Alq₃ molecule has three 8-hydroxyquinoline ligands perpendicular to each other, the probability is large for one cobalt atom to be stopped by collision with an Alq₃ molecule. As a result, penetration depth of cobalt atom is limited to about 2 nm, even with the highest initial energy.

At its final position in each trajectory, the cobalt atom is located near one aromatic ring in an Alq₃ molecule, because aromatic rings are more attractive for cobalt atoms compared to O or N atoms according to our DFT calcu-

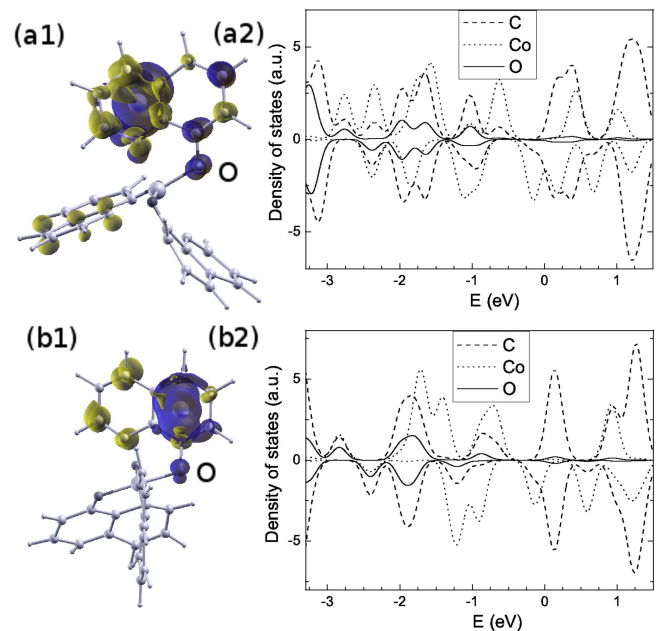


FIG. 5. (Color Online) Two different final positions of cobalt with respect to Alq₃ molecule: (a1) and (b1), spin density $\rho_{\uparrow}(\vec{r}) - \rho_{\downarrow}(\vec{r})$ contour plots, positive for blue (heavy gray) and negative for yellow (light gray); and (a2) and (b2), projected density of states for two Alq₃-Co clusters: dash line for carbon, dot line for cobalt and solid line for oxygen. In (a1) and (b1), oxygen atoms are labeled.

lations results. To obtain the electronic structure of Co-doped Alq₃ molecules, the cobalt atom and the nearest Alq₃ molecule are extracted to form an Alq₃-Co cluster. Geometries, spin density, and projected density of states (PDOS) for two typical Alq₃-Co clusters are shown in Fig. 5. For one cluster [Fig. 5(a)] the cobalt atom is located near the center of a C-N ring, but in the other cluster [Fig. 5(b)] it is near the center of a C₆ ring. In both the cases, the magnetic moments of the cobalt atom were calculated to be $+1.0 \mu_B$. Spin-down electrons, with spin is antiparallel to that of cobalt atom, accumulate near the C-N ring in the 8-hydroxyquinoline ligand in contact with the cobalt atom, while the oxygen atom has positive magnetic moment, as shown in Fig. 5(a1)(b1). In both cases, PDOS of carbon and oxygen atoms show exchange splitting of spin-up and spin-down channels around -1 eV and around -2.5 eV, as shown in Fig. 5(a2) and Fig. 5(b2), which indicates indirect interactions between cobalt atom and oxygen atom through the aromatic rings³⁹. The atomic charge on the cobalt atom in both cases was calculated using the Bader charge analysis method⁴⁰ to be $+0.56$, which is consistent with previous DFT calculations.²⁴

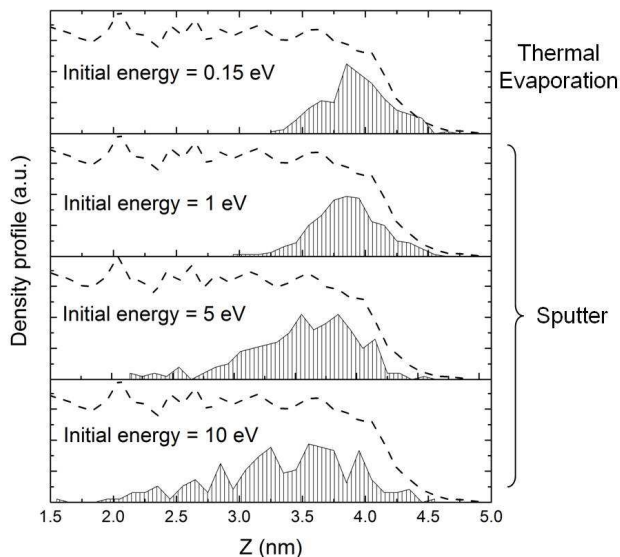


FIG. 6. Density profiles of carbon (dashed lines) and cobalt (shadow) elements in arbitrary units for different cobalt initial energies. The corresponding experimental deposition methods are shown.

IV. SUMMARY AND OUTLOOK

In summary, using density functional theory and molecular dynamics simulations, we studied the deposition of cobalt atoms onto Alq_3 films. A density functional theory calibrated force field was constructed to describe interaction between cobalt atom and Alq_3 molecule. Statistics on penetration depths of cobalt atoms and its dependence on initial kinetic energy were obtained. A cobalt atom with low initial energy (0.15 eV) penetrates little, but stays near the surface of the Alq_3 thin film. However, a cobalt atom with high initial energy (1, 5, 10 eV) could penetrate more into the Alq_3 . The penetration depth of the cobalt atom is limited to about 2 nm. Microscopic analysis of the cobalt atom trajectory shows that the injected cobalt atom loses its kinetic energy through collision with 8-hydroxyquinoline ligands of the Alq_3 molecules which are not parallel to velocity of

the cobalt atom. Additionally, orbital hybridizations of carbon and oxygen atoms due to cobalt atoms and sizable charge transfer from cobalt atoms to their nearest neighboring Alq_3 molecule were revealed by density functional theory calculations.

In order to provide direct comparison to experimental observation of metal penetration by EELS technique,¹⁸ the density profiles of carbon and cobalt elements along the z-axis for different initial energies are illustrated in Fig. 6. As shown in Fig. 6, the intermixing of Co atoms with Alq_3 molecules cannot be avoided but limited to a few layers of Alq_3 near the interface, and the amount of intermixing can be minimized if Co atoms were deposited with the lowest kinetic energy, e.g., using thermal evaporation method.

The indirect deposition method used in Ref. 41, and the buffer layer assisted growth method used in Ref. 17, and firm-up of organic layer by heating used in Ref. 15 are efficient approaches to minimize the intermixing at interfaces, although they are complex and suffer from low product yield. However, it was proposed that the formation of ill-defined interface does not result from the inclusion of metal atoms in organic layers.²² In the presence of pinholes and grains in Alq_3 thin films, one possible approach to bypass the ill-defined interface problem is to fabricate nanoscale junctions with small enough cross section (e.g., $< 50 \times 50 \text{ nm}^2$)^{22,42}, or even to fabricate single-molecule magnetic tunnel junctions.

ACKNOWLEDGMENTS

The project was supported by the State Key Project of Fundamental Research of Ministry of Science and Technology [MOST, No. 2010CB934400] and National Natural Science Foundation of China [NSFC, Grant No. 10934099, 51021061, and 10911130234], and US DOE/BES DE-FG02-02ER45995 (H.-P. Cheng) and the partial support of K. C. Wong Education Foundation, Hong Kong. The calculations were performed on NERSC computers. A portion of this research was conducted at the Center for Nanophase Materials Sciences, which is sponsored at Oak Ridge National Laboratory by the Scientific User Facilities Division, Office of Basic Energy Sciences, U.S. Department of Energy.

¹ R. H. Friendand, R. W. Gymer, A. B. Holmes, J. H. Burroughes, R. N. Marks, C. Taliani, D. D. C. Bradley, D. A. D. Santos, J. L. Brédas, M. Lögdlund, and W. R. Salaneck, *Nature (London)* **397**, 121 (1999).

² Z. H. Xiong, D. Wu, Z. V. Vardeny, and J. Shi, *Nature (London)* **427**, 821 (2004).

³ G. Fisher, A. Walker, A. Hooper, T. Tighe, K. Bahnck, H. Skriba, M. Reinard, B. Haynie, R. Opila, N. Winograd, and D. Allara, *J. Am. Chem. Soc.* **124**, 5528 (2002).

⁴ A. Walker, T. Tighe, O. Cabarcos, M. Reinard, B. Haynie,

S. Uppili, N. Winograd, , and D. Allara, *J. Am. Chem. Soc.* **126**, 3954 (2004).

⁵ Z. Zhu, T. Daniel, M. Maitani, O. Cabarcos, D. Allara, and N. Winograd, *J. Am. Chem. Soc.* **128**, 13710 (2006).

⁶ H. Ahn and J. Whitten, *J. Phys. Chem. B* **107**, 6565 (2003).

⁷ G. Nagy and A. Walker, *J. Phys. Chem. B* **110**, 12543 (2006).

⁸ A. Walker, T. Tighe, O. Cabarcos, B. Haynie, D. Allara, and N. Winograd, *J. Phys. Chem. C* **111**, 765 (2007).

- ⁹ P. Lu, K. Demirkan, R. Opila, , and A. Walker, *J. Phys. Chem. C* **112**, 2091 (2008).
- ¹⁰ P. Lu and A. Walker, *Langmuir* **23**, 12577 (2007).
- ¹¹ S. Alkis, C. Cao, H.-P. Cheng, and J. L. Krause, *J. Phys. Chem. C* **113**, 6360 (2009).
- ¹² S. Alkis, J. L. Krause, J. N. Fry, and H.-P. Cheng, *Phys. Rev. B* **79**, 121402 (2009).
- ¹³ R. Giro and M. J. Caldas, *Phys. Rev. B* **76**, 161303 (2007).
- ¹⁴ R. Giro and M. J. Caldas, *Phys. Rev. B* **78**, 155312 (2008).
- ¹⁵ T.-X. Wang, H.-X. Wei, Z.-M. Zeng, X.-F. Han, Z.-M. Hong, and G.-Q. Shi, *Appl. Phys. Lett.* **88**, 242505 (2006).
- ¹⁶ D. Liu, Y. Hu, H. Guo, and X.-F. Han, *Phys. Rev. B* **78**, 193307 (2008).
- ¹⁷ D. Sun, L.-F. Yin, C.-J. Sun, H.-W. Guo, Z. Gai, X.-G. Zhang, T. Z. Ward, Z.-H. Cheng, and J. Shen, *Phys. Rev. Lett.* **104**, 236602 (2010).
- ¹⁸ H. Vinzelberg, J. Schumann, D. Elefant, R. B. Gangineni, J. Thomas, and B. Büchner, *J. Appl. Phys.* **103**, 093720 (2008).
- ¹⁹ T. S. Santos, J. S. Lee, P. Migdal, I. C. Lekshmi, B. Satpati, and J. S. Moodera, *Phys. Rev. Lett.* **98**, 016601 (2007).
- ²⁰ W. H. Xu, J. Brauer, G. Szulczewski, M. S. Driver, and A. N. Caruso, *Appl. Phys. Lett.* **94**, 233302 (2009).
- ²¹ F. Borgatti, I. Bergenti, F. Bona, V. Dediu, A. Fondacaro, S. Huotari, G. Monaco, D. A. MacLaren, J. N. Chapman, and G. Panaccione, *Appl. Phys. Lett.* **96**, 043306 (2010).
- ²² L. Lin, Z.-Y. Pang, F.-G. Wang, M.-S. Lv, T.-L. Yang, L.-N. Ye, and S.-H. Han, *Appl. Surf. Sci.* **255**, 5682 (2009).
- ²³ J. M. Baik, Y. Shon, S. J. Lee, Y. H. Jeong, T. W. Kang, and J.-L. Lee, *J. Am. Chem. Soc.* **130**, 13522 (2008).
- ²⁴ F. G. Wang, Z. Y. Pang, L. Lin, S. J. Fang, Y. Dai, and S. H. Han, *Appl. Phys. Lett.* **96**, 053304 (2010).
- ²⁵ A. K. Rappe, C. J. Casewit, K. S. Colwell, W. A. Goddard, and W. M. Skiff, *J. Am. Chem. Soc.* **114**, 10024 (1992).
- ²⁶ A. K. Rappé and W. A. Goddard, *J. Phys. Chem.* **95**, 3358 (1991).
- ²⁷ W. Kohn and L. J. Sham, *Phys. Rev.* **140**, A1133 (1965).
- ²⁸ P. Giannozzi, S. Baroni, N. Bonini, M. Calandra, R. Car, C. Cavazzoni, D. Ceresoli, G. L. Chiarotti, M. Cococcioni, I. Dabo, A. Dal Corso, S. de Gironcoli, S. Fabris, G. Fratesi, R. Gebauer, U. Gerstmann, C. Gougousis, A. Kokalj, M. Lazzeri, L. Martin-Samos, N. Marzari, F. Mauri, R. Mazzarello, S. Paolini, A. Pasquarello, L. Paulatto, C. Sbraccia, S. Scandolo, G. Sclauzero, A. P. Seitsonen, A. Smogunov, P. Umari, and R. M. Wentzcovitch, *Journal of Physics: Condensed Matter* **21**, 395502 (19pp) (2009).
- ²⁹ J. P. Perdew, K. Burke, and M. Ernzerhof, *Phys. Rev. Lett.* **77**, 3865 (1996).
- ³⁰ P. E. Blöchl, *Phys. Rev. B* **50**, 17953 (1994).
- ³¹ G. Kresse and D. Joubert, *Phys. Rev. B* **59**, 1758 (1999).
- ³² W. Tang, E. Sanville, and G. Henkelman, *J. Phys.: Condens. Matter* **21**, 084204 (2009).
- ³³ A. Lukyanov, C. Lennartz, and D. Andrienko, *Phys. Status Solidi A* **206**, 2737 (2009).
- ³⁴ D. Dhandapani, N. A. Morley, M. R. J. Gibbs, T. Kreouzis, P. Shakya, P. Desai, and W. P. Gillin, *IEEE Trans. Magn.* **46**, 1307 (2010).
- ³⁵ A. A. Sidorenko, C. Pernechele, P. Lupo, M. Ghidini, M. Solzi, R. D. Renzi, I. Bergenti, P. Graziosi, V. Dediu, L. Hueso, and A. T. Hindmarch, *Appl. Phys. Lett.* **97**, 162509 (2010).
- ³⁶ I. Bergenti, A. Riminucci, E. Arisi, M. Murgia, M. Cavallini, M. Solzi, F. Casoli, and V. Dediu, *J. Magn. Magn. Mater.* **316**, e987 (2007).
- ³⁷ K. Seshan, ed., *Handbook of Thin-Film Deposition Processes and Techniques: Principles, Methods, Equipment and Applications*, 2nd ed. (William Andrew Publishing/Noyes, 2002).
- ³⁸ W. Smith, C. Yong, and P. Rodger, *Molecular Simulation* **28**, 385 (2002).
- ³⁹ L. Lin, Z.-Y. Pang, S.-J. Fang, F.-G. Wang, S.-M. Song, Y.-Y. Huang, X.-J. Wei, . H.-S. Yu, and S.-H. Han, *J. Phys. Chem. A* **115**, 880 (2011).
- ⁴⁰ W. Tang, E. Sanville, and G. Henkelman, *J. Phys.: Condens. Matter* **21**, 084204 (2009).
- ⁴¹ S. Wang, Y.-J. Shi, L. Lin, B.-B. Chen, F.-J. Yue, J. Du, H.-F. Ding, F.-M. Zhang, and D. Wu, *Synt. Mat.* **161**, 1738 (2011).
- ⁴² C. Barraud, P. Seneor, R. Mattana, S. Fusil, K. Bouzehouane, C. Deranlot, P. Graziosi, L. Hueso, I. Bergenti, V. Dediu, F. Petroff, and A. Fert, *Nat. Phys.* **6**, 615 (2010).